https://ntrs.nasa.gov/search.jsp?R=19720013235 2020-03-23T10:51:56+00:00Z

ABORT SEPARATION OF THE SHUTTLE

John P. Decker, LRC; Kenneth L. Blackwell, Joseph L. Sims, MSFC;
R. H. Burt, W. T. Strike, Jr., ARO;
C. Donald Andrews, L. Ray Baker, Jr., LMSC-Huntsville;
John M. Rampy, Northrop-Huntsville

ABORT

(Figure 1)

During the past year, the abort situation as applied to the Phase B shuttle concepts has been clarified somewhat. Many sub-systems were being designed to accept failures. Consequently, three distinct failure modes, catastrophic, critical, and non-critical, were defined. In the case of a catastrophic failure, both vehicles would be lost. Possibly the crew of each vehicle would be saved by some type of an escape system. For non-critical failures, the abort mode for the booster would be to deplete the excess propellant by burning the main propulsion engines and conducting staging operations near nominal conditions. The booster would return to the launch site after separation while the orbiter would have a trajectory tailored to abort once around and return to the launch site or a suitable downrange recovery site.

For critical aborts when mated flight would not be possible the stages would have to separate at off nominal conditions, that is, perform an abort separation maneuver in the sensible atmosphere. After separation both the orbiter and booster trajectories would be tailored so that both vehicles could land at a suitable site. The question here is, can the vehicles safely perform an abort separation maneuver at conditions from lift-off to nominal staging and if this is feasible, how does this influence the abort philosophy?

The abort separation work that will be discussed in this presentation has been an intercenter, interagency and intergovernmental effort and is the reason for the number of co-authors on the paper. In this paper the overall effort and what has been learned about abort separation of the shuttle will be discussed.

ABORT

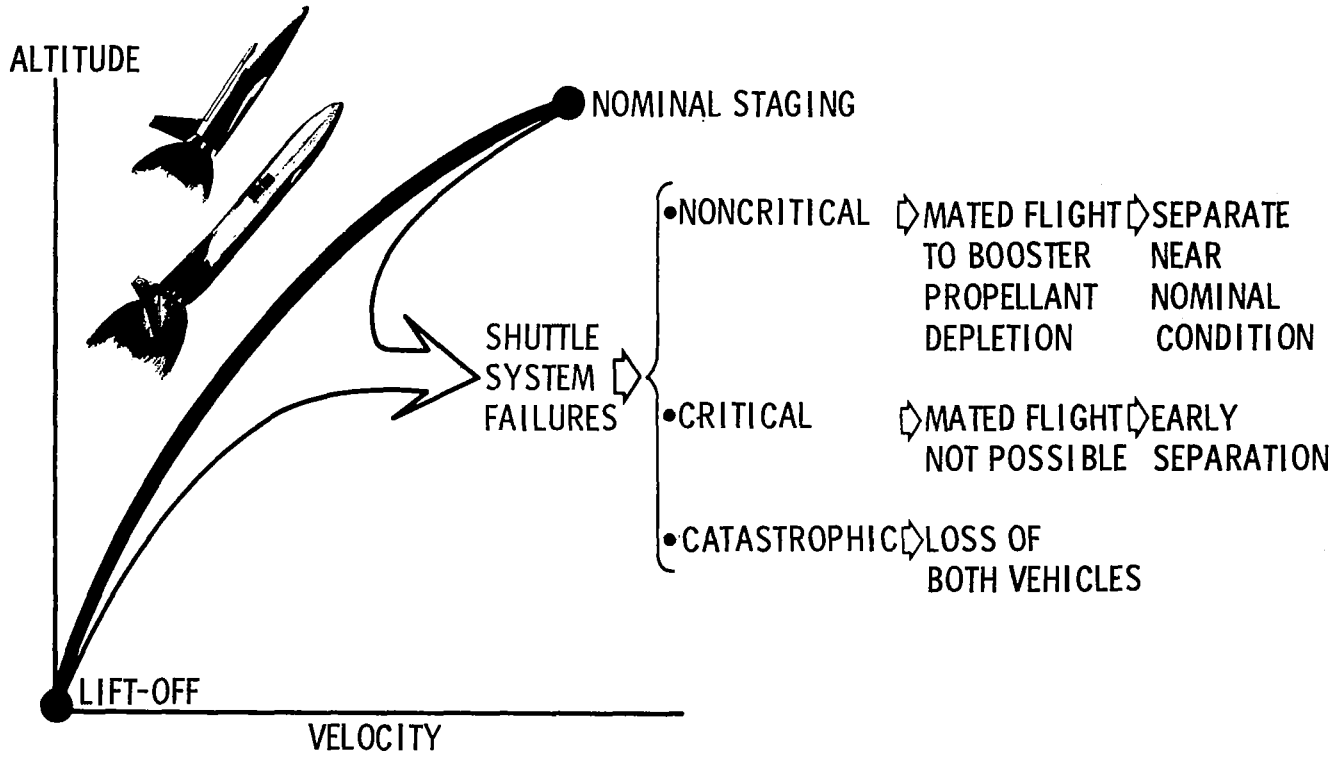

Figure 1

110T

STAGING STUDIES DURING THE SIXTIES

(Figure 2)

Numerous staging studies (references 1 - 17) were conducted in the sixties on the vehicles shown in this figure. These staging studies were preliminary and consequently a clear answer to the question of parallel separation of two vehicles of similar size was not obtained. In fact, staging in the sensible atmosphere for most of these vehicle systems was generally avoided since some of the preliminary results indicated that staging in the sensible atmosphere would be difficult.

The parallel separation of two vehicles of similar size is different than the separation problem for any system designed up to the present. For the shuttle we are interested in the integrity of both vehicles at separation. For previous systems, only the integrity of the upper stage was involved at separation. Furthermore, the separation problem of the shuttle is also different than separating an external store from a parent vehicle such as the X-15 from the B-52. In the case of the separation of an external store, only the external store aerodynamic characteristics are disturbed from nominal conditions. For the parallel separation of two vehicles of similar size, both vehicles' aerodynamic characteristics are disturbed from nominal conditions.

STAGING STUDIES DURING THE SIXTIES

1963 - BOEING

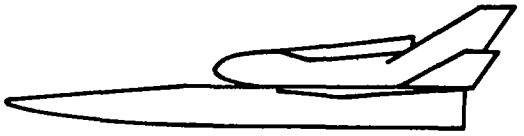

1967 - LaRC

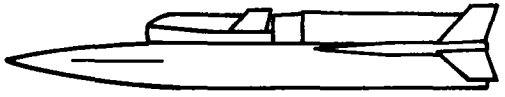

1964 - LaRC

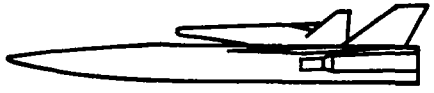

1969 - AFFDL

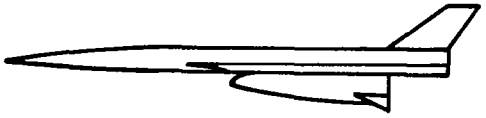

1966 - AFFDL

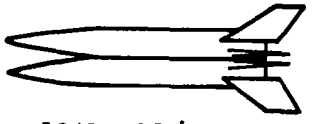

1969 - GD/C

Figure 2

ABORT STAGING TECHNOLOGY CONSIDERATIONS

(Figure 3)

Many disciplines must be considered in an abort analysis and many iterations will take place between the disciplines before a workable abort procedure is completed. However, it is not necessary to close all these loops to accomplish the objectives of this study which were to perform a sensitivity analysis of factors which affect a successful abort maneuver and to provide guidelines for future studies.

The approach was to conduct wind tunnel tests using the best simulation techniques and data acquisition-analysis-dissemination procedures that were available within time and facility limitations. Static stability, dynamic stability and local loads investigations were conducted during this study. These results were extensively utilized in the dynamic simulation computer program which integrates the equations of motion for both vehicles (6 degrees of motion for each) and calculates their relative position and attitude. In the present effort only the longitudinal motion was studied in depth. Close coordination was maintained in planning and conducting of these tests to assure that data required for calculating separation trajectories would be available in an optimum format and on a timely schedule. Information from other disciplines such as mass characteristics, propulsion characteristics, mechanism kinematics, ascent conditions, and thrust vector control authority were obtained as open loop inputs from phase B studies while the aero control authority was looked at during the wind tunnel tests. The underlined items therefore are the items that were considered in the dynamic simulation program. The other items have been looked at to various degrees by other researchers.

ABORT STAGING TECHNOLOGY CONSIDERATIONS

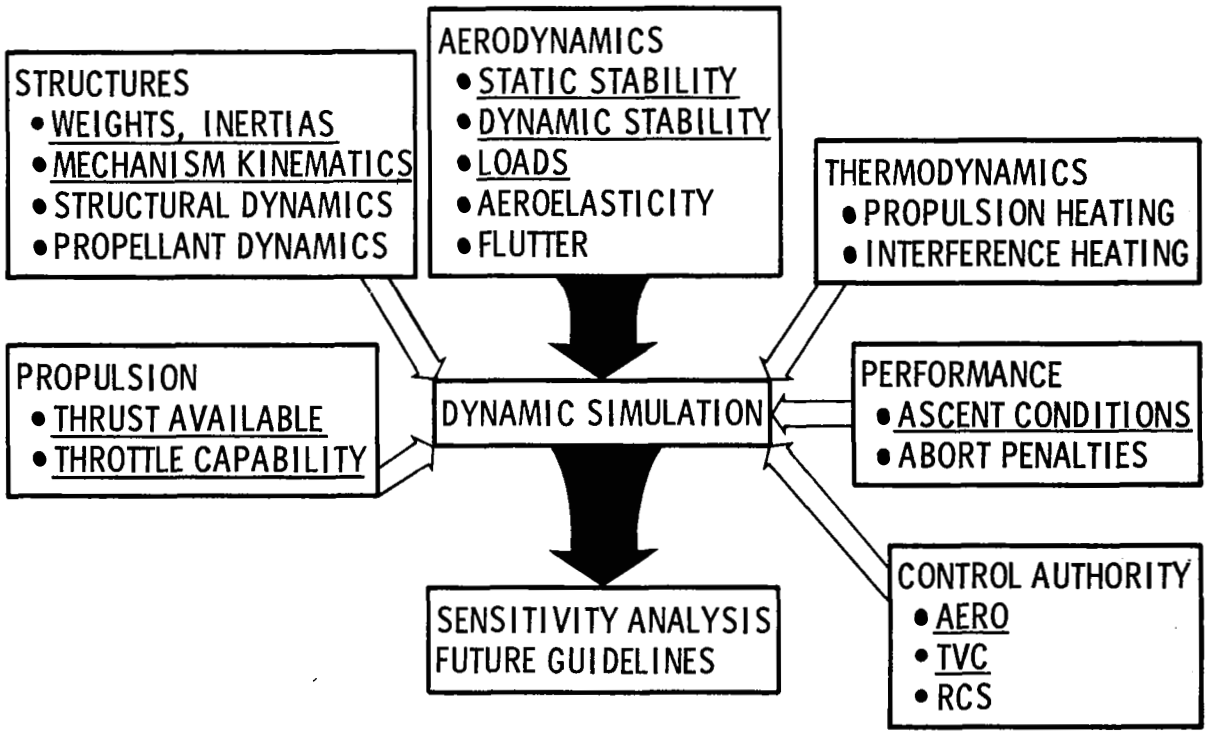

Figure 3

FORCE AND MOMENT TESTS AND PRESSURE DISTRIBUTION TESTS

(Figure 4)

Both the static stability and local loads investigations were conducted at Mach numbers from 2 to 6 in tunnel A of the von Kármán Gas Dynamics Facility at the Arnold Engineering Development Center. The vehicle system selected for these investigations was the McDonnell Douglas Corporation's Phase B shuttle concept. For the static stability tests, both stages were instrumented with strain gage balances to measure the forces and moments that occur on each vehicle when in proximity to each other. For the local loads investigation, the booster and orbiter were instrumented with pressure orifices to measure the local interference loads on the vehicles. All tests were conducted simulating the rocket exhaust plume from both the orbiter and booster. The two-engine orbiter arrangement and the twelve-engine booster arrangement were each simulated by a toroidal model nozzle, details of which are described in figures 6 - 9. The plume was simulated at various altitudes corresponding to the Mach number range investigated. The dynamic pressure for these conditions ranged from about 19,152 N/m^2 (400 psf) at M = 2 to 1,436 N/m^2 (30 psf) at M = 6.

Nominal staging conditions, references 18 and 19, have been looked at by Marshall Space Flight Center and Manned Spacecraft Center. The Mach number 1 regime has also been looked at in some depth by both Manned Spacecraft Center and General Dynamics/Convair. Other related staging data are shown in reference 20.

FORCE AND MOMENT AND PRESSURE DISTRIBUTION TESTS

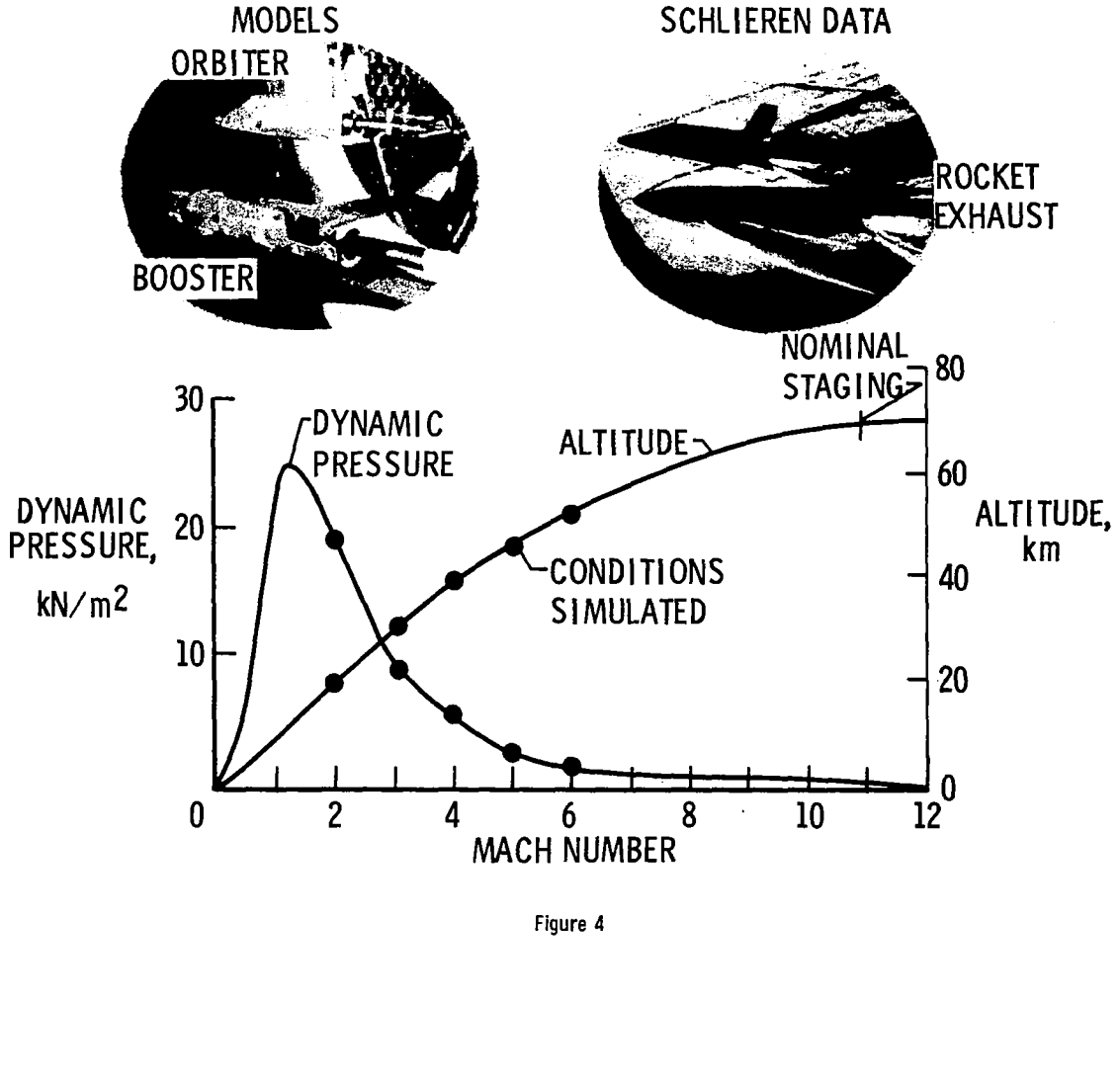

Figure 4

AERODYNAMIC DATA MATRIX

(Figure 5)

The matrix for which aerodynamic interference data was obtained is shown in this figure. Each dot represents the placement of the orbiter center of gravity with respect to booster center of gravity. An automatic control system allowed a series of orbiter positions to be programmed prior to a test run. This control system was integrated with the data recording system and angle-of-attack system so that model positioning, pitching, and data recording were completely automatic once a matrix was initiated. The orbiter and booster were pitched together as a unit from -10 to +10°. For the force and moment tests the data was recorded in a continuous pitch mode while for the pressure distribution tests the data was recorded in a pitch-pause mode. The orbiter incidence angle was varied by manual adjustment and incidences angles of 0°, $\pm$5°, and $\pm$10° were investigated. Orbiter thrust levels of 0%, 25%, 50%, and 100% and booster thrust levels of 0%, 50%, and 100% were investigated. By making use of the automatic control system 1850 pitch polars were obtained during the force and moment tests and 300 pitch polars were obtained during the pressure tests in 100 hr of tunnel occupancy time. All of the force and moment pitch polars were subsequently used in the dynamic simulation program.

AERODYNAMIC DATA MATRIX

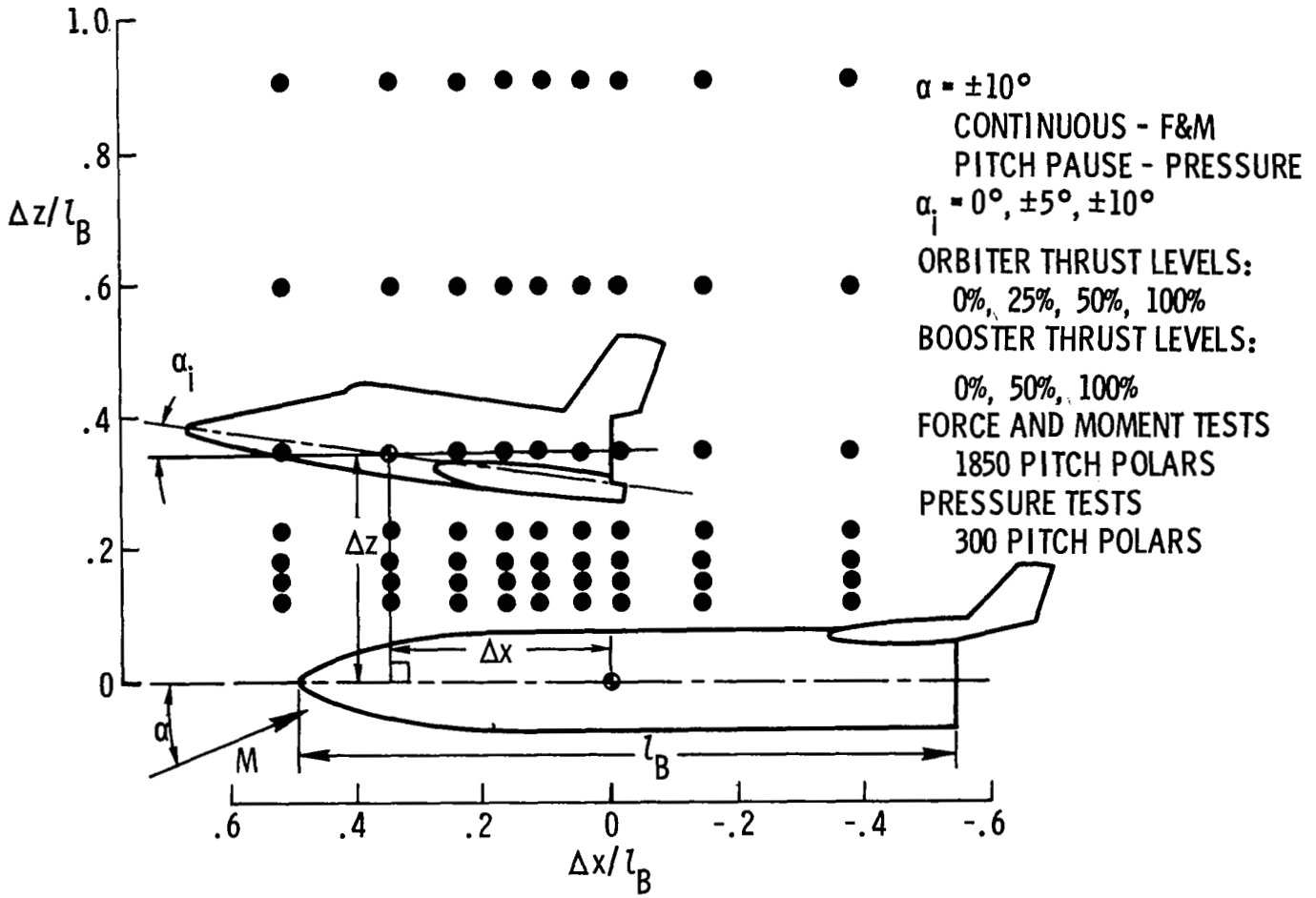

Figure 5

ROCKET EXHAUST SIMULATION

(Figure 6)

When a complex flow field such as a rocket's exhaust plume is to be modeled, it is usually impossible to simulate all of the gas dynamic parameters over the entire flow field if a different gas must be used. Thus, it is necessary to identify the important physical phenomena and the similarity parameters that control them. The two major effects of the plume on the flow field which need to be simulated are shown in this figure. These two effects are best simulated when the size and shape of the exhaust plume are scaled from the full scale plume. This is achieved by use of the similarity equations obtained from reference 21.

ROCKET EXHAUST SIMULATION

MAJOR PLUME EFFECTS TO BE MODELED

- AERODYNAMIC LOADS CAUSED BY THE PLUME GENERATED SHOCK LAYER
- LOADS CAUSED BY DIRECT PLUME IMPINGEMENT

PLUME PARAMETER SIMULATION TO ACHIEVE ABOVE RESULTS

- EXHAUST PLUME SIZE
- EXHAUST PLUME SHAPE

SIMILARITY EQUATIONS

$$\left(\frac{M_1}{\gamma}\right)_{MODEL} = \left(\frac{M_1}{\gamma}\right)_{FULL\ SCALE}$$

$$\left(\delta_J\right)_{MODEL} = \left(\delta_J\right)_{FULL\ SCALE}$$

$$\left(\theta_N\right)_{MODEL} = \left(\theta_N\right)_{FULL\ SCALE}$$

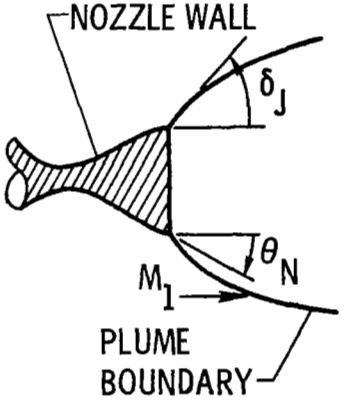

Figure 6

ESTIMATED FULL SCALE PLUME PARAMETERS

(Figure 7)

Two of the full scale plume parameters for the orbiter engine used in the similarity relationships are presented over the altitude range of interest. These two parameters are the plume boundary angle at the engine exit plane and the plume boundary Mach number. These results were computed for the combustion products of O_2/H_2 in thermodynamic equilibrium. The gas mixture has a variable ratio of specific heats over the range of temperatures in the nozzle and plume. Therefore, if the full scale similarity parameters are to be reproduced by a gas with a constant ratio of specific heats, the model nozzle area ratio will vary with altitude.

ESTIMATED FULL SCALE PLUME PARAMETERS
ORBITER ENGINE

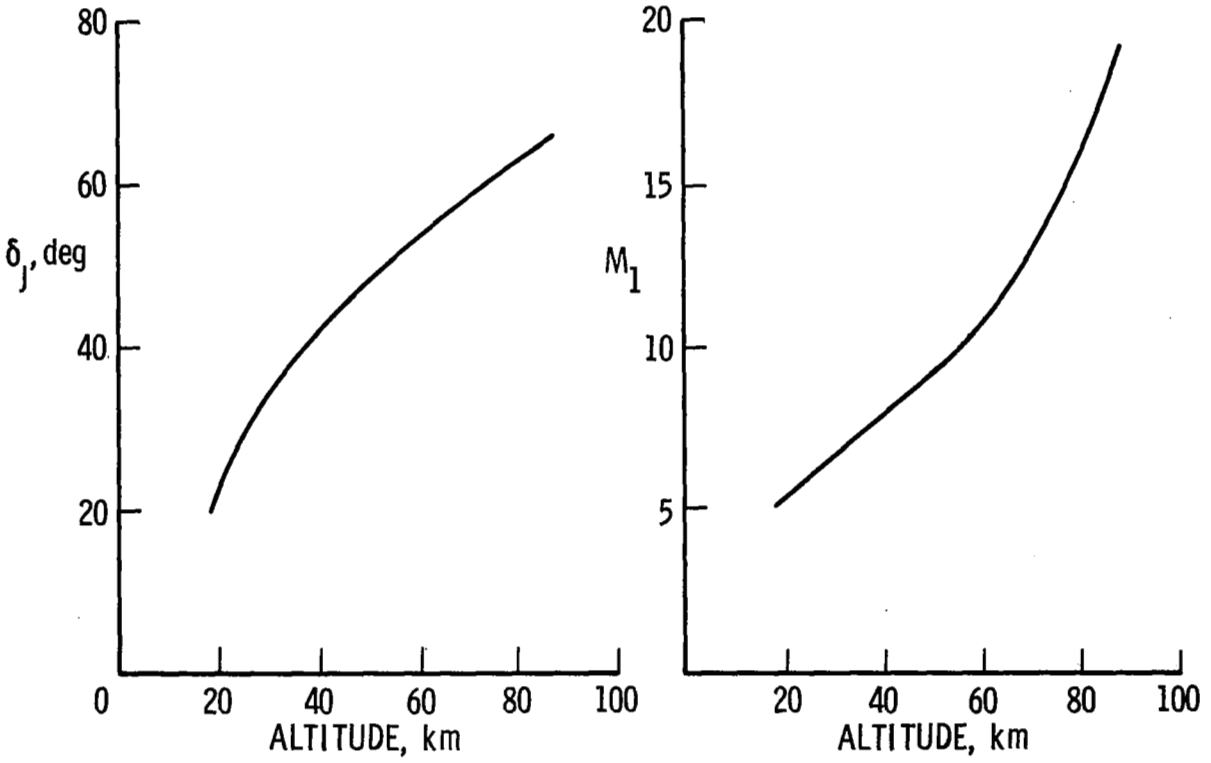

Figure 7

MODEL PLUME CHARACTERISTICS

(Figure 8)

The requirements for varying area ratio and hardware restraints imposed by the support stings led to the design of a toroidal model nozzle for both the orbiter and booster. Both nozzles were similar in detail. The support sting served as the center body of the nozzle and also as a conduit for the air supply to the nozzles. The nozzle area ratio, which is the ratio of the exit area to the throat area, could be varied by a longitudinal translation of the outer wall in relation to the inner body.

The required area ratio variation of the orbiter nozzle over this altitude range is shown. A calibration of the model nozzles was performed (reference 22) in order to establish the operating characteristics as a function of geometric setting. This was accomplished by computing the nozzle area ratio from exit plane static pressure data and from plume angles at the nozzle lip. These results are also shown and agree well enough so that we were confident that the required plumes would be generated by the nozzles.

MODEL PLUME CHARACTERISTICS

ORBITER ENGINE

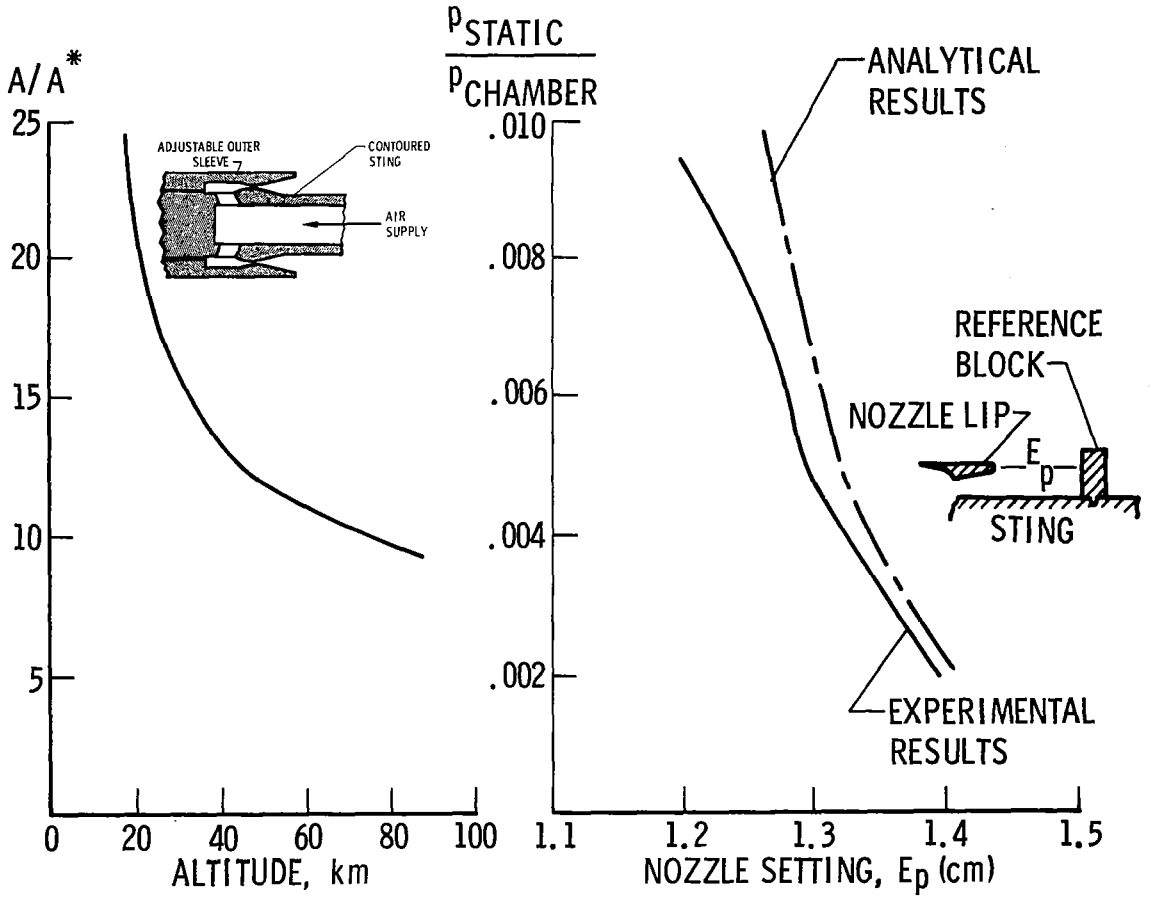

Figure 8

EXTERNAL FLOW FIELD EFFECTS

(Figure 9)

To illustrate how the rocket exhaust influences the vehicles and also the importance of an external stream, representative data obtained during the pressure distribution tests are presented in this figure. Two plume impingement conditions are illustrated. One is where there is no external flow and the other is for an external Mach number 5 stream. The orbiter nozzle area ratio and chamber pressure are the same in both cases. The plume boundaries as viewed in the pitch plane of the vehicles did not differ by more than 5 or 6 percent at the orbiter nozzle exit.

The centerline peak pressures were nearly equal for the two cases illustrated and these peaks occurred at nearly the same booster model station. The important difference here is that the plume impingement disturbance propagates laterally or further outboard along the wing surface when the external stream is present. This is probably due to the combined wakes of the orbiter and booster interacting with the orbiter plume and causing the plume induced impingement pressure distribution to expand further in the yaw plane when the external Mach number 5 stream is present.

EXTERNAL FLOW FIELD EFFECTS

$\Delta x/l_B = 0.104$; $\Delta z/l_B = 0.150$; $\alpha = 0°$; $\alpha_i = 5°$; ORBITER POWER = 100%

SCHLIEREN DATA

NO EXTERNAL FLOW

EXTERNAL FLOW
M = 5

BOOSTER ISOBARS

NO EXTERNAL FLOW

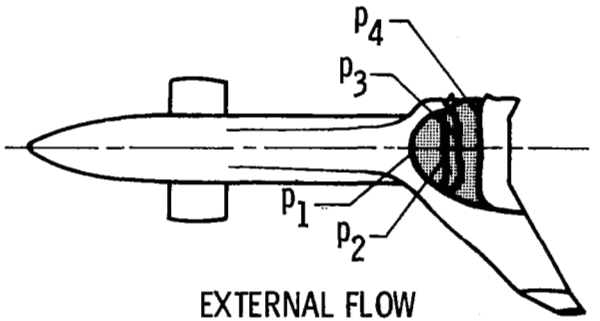

EXTERNAL FLOW
M = 5

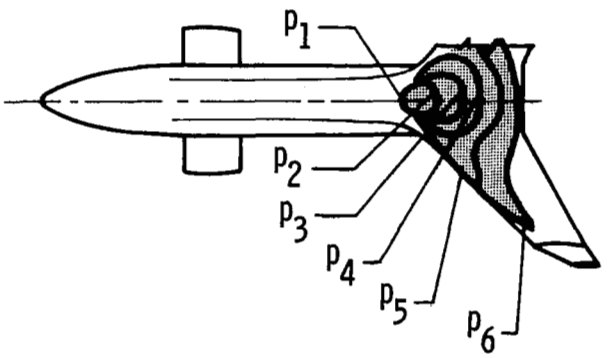

Figure 9

EFFECT OF ORBITER POWER LEVEL

(Figure 10)

An important feature learned about the use of simulated engine propulsion in conjunction with abort staging wind tunnel tests was that increments in aerodynamic coefficients for the booster as a function of orbiter engine power level were linear over large portions of the orbiter power range. This is illustrated in this figure where the increments on the booster aerodynamic coefficients for a representative position and attitude of the orbiter are shown as a function of orbiter power setting. The linearization of the curves is significant when considering application of the data to a flight dynamic simulation program where power transients must be considered. Data required for basic attitude and position variations for the separation envelope are already voluminous so the addition of another major variable requiring detailed definition would only complicate the study of abort staging and increase costliness of data acquisition. From what has been learned during this investigation it is envisioned that for final design data only a few (3, 4) power settings would be required to be tested for each of the other test condition variables.

EFFECT OF ORBITER POWER LEVEL

$M = 5; \Delta x/l_B = 0.104; \Delta z/l_B = 0.151; \alpha = 0°; \alpha_i = 5°$

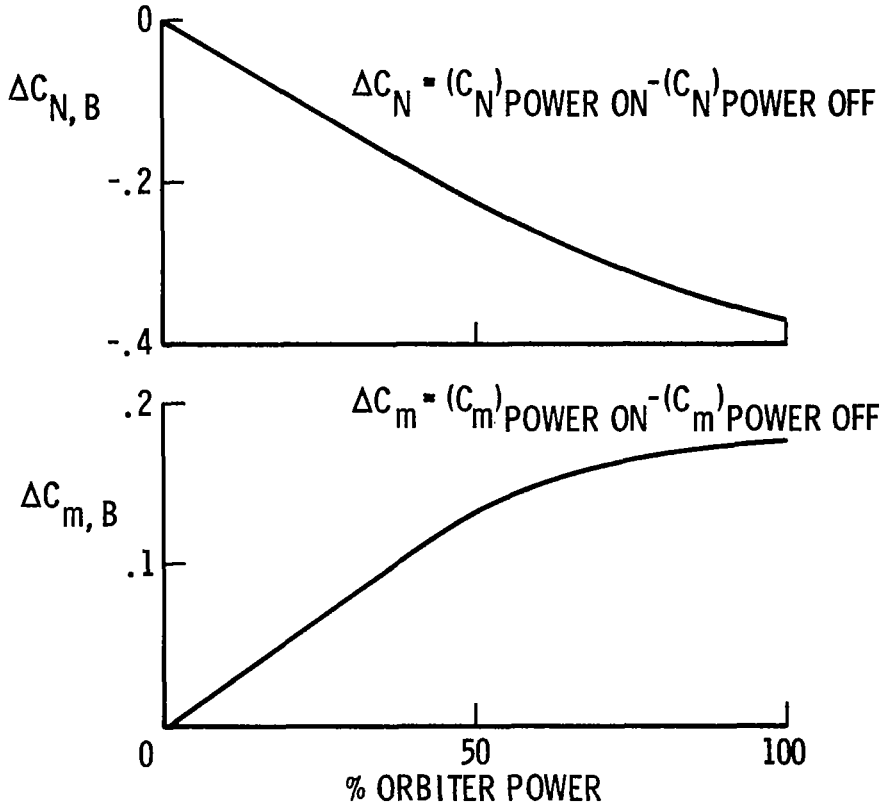

Figure 10

LOCUS OF MEASURED INTERFERENCE EFFECTS

(Figure 11)

The locus of measured interference effects as a function of the position parameters (figure 5) on the orbiter and booster due to the proximity of the other vehicle is illustrated in this figure at Mach numbers of 2, 3, and 5. The three interference conditions shown are an interference free condition, an aerodynamic interference condition where the interferences are due to mutual shock impingement on each vehicle, and a propulsive interference condition due to the impingement of the rocket exhaust plumes.

As the Mach number is increased, the region where the orbiter is at interference free conditions becomes larger due to the bow shock of the booster bending further towards the booster body. At the same time the region where the rocket exhaust from the booster impinges on the orbiter becomes larger since the plume of the booster becomes larger. Similar trends are also shown for the booster except that the regions are reversed as would be expected.

LOCUS OF MEASURED INTERFERENCE EFFECTS

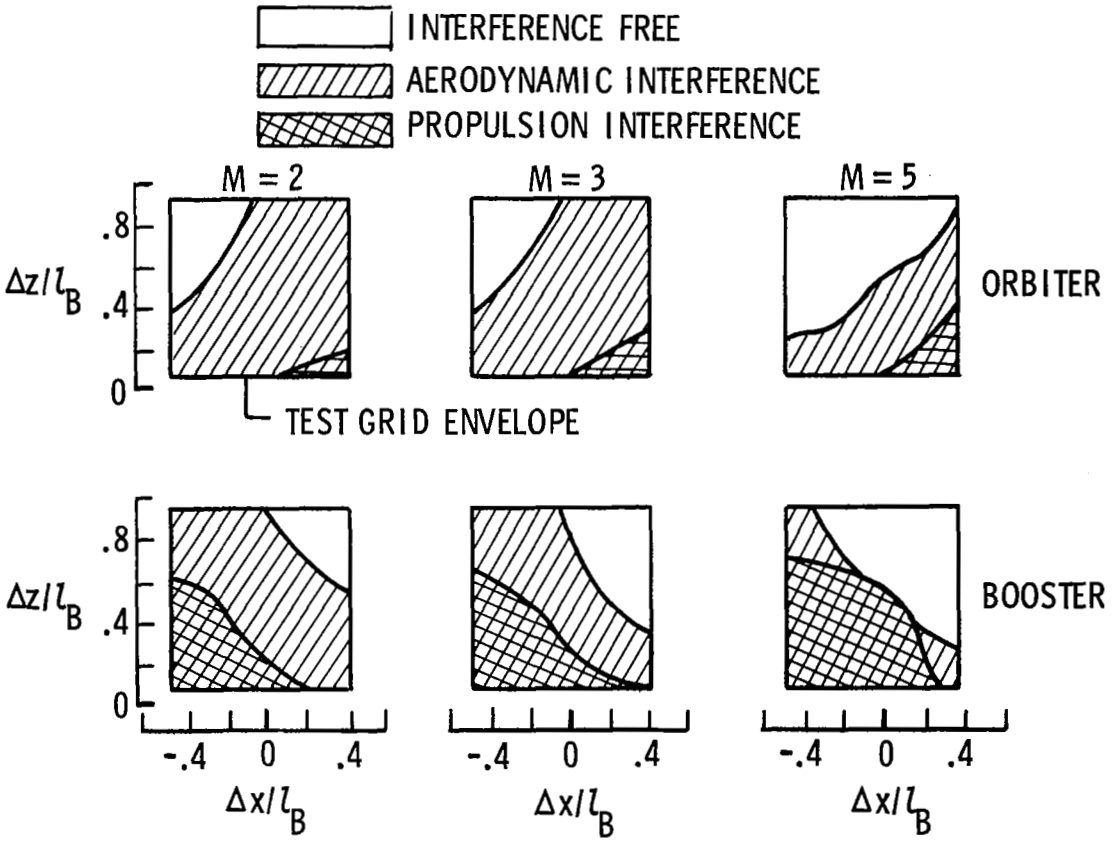

Figure 11

CENTERLINE PRESSURE DISTRIBUTIONS

(Figure 12)

The complexity of the flow fields is illustrated in this figure where the centerline pressure distributions on the orbiter and booster are shown as a function of distance from the nose of each vehicle. Two curves are illustrated. One is the interference free curve for the orbiter and booster and the other is for the orbiter in proximity to the booster and with the orbiter power level at 100% and the booster power level at 50%. The increase in centerline static pressures on the orbiter is due to the booster bow wave impingement and the canard bow wave impingement. No plume impingement is shown on the orbiter since for this case the orbiter is forward of the booster base. For the booster the increase in centerline static pressures is due to the orbiter bow wave impingement, the location of the booster canard, and the orbiter plume impingement. The important fact on this figure is the influence of the booster canard on the loadings of both the orbiter and booster and the orbiter plume effects.

CENTERLINE PRESSURE DISTRIBUTIONS

$M = 3$; $\Delta x/\ell_B = 0.227$; $\Delta z/\ell_B = .120$; $\alpha = 0^0$; $\alpha_i = 0^0$

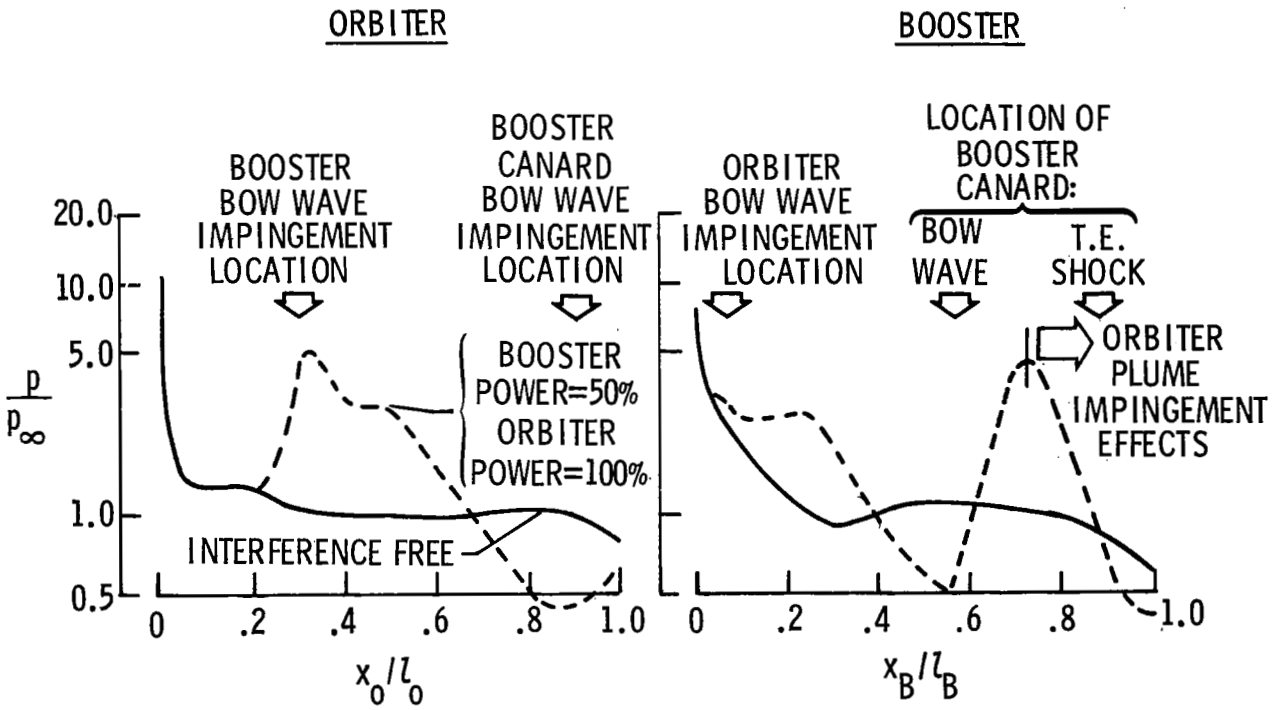

Figure 12

EFFECT OF BOOSTER CANARD

(Figure 13)

The effect of the booster canard on the proximity aerodynamics is shown in this figure at a Mach number of 3. The two curves illustrated are for the canard on and canard off and it is seen that the canard significantly changes the forces and moments on both vehicles, thus confirming that the proximity aerodynamic data is not only dependent on Mach number, rocket exhaust impingement, and relative position and attitudes of the stages, but also dependent on configuration.

EFFECT OF BOOSTER CANARD

$M = 3; \Delta x/l_B = 0.104; \Delta z/l_B = 0.120$

ORBITER POWER = 100%; BOOSTER POWER = 50%

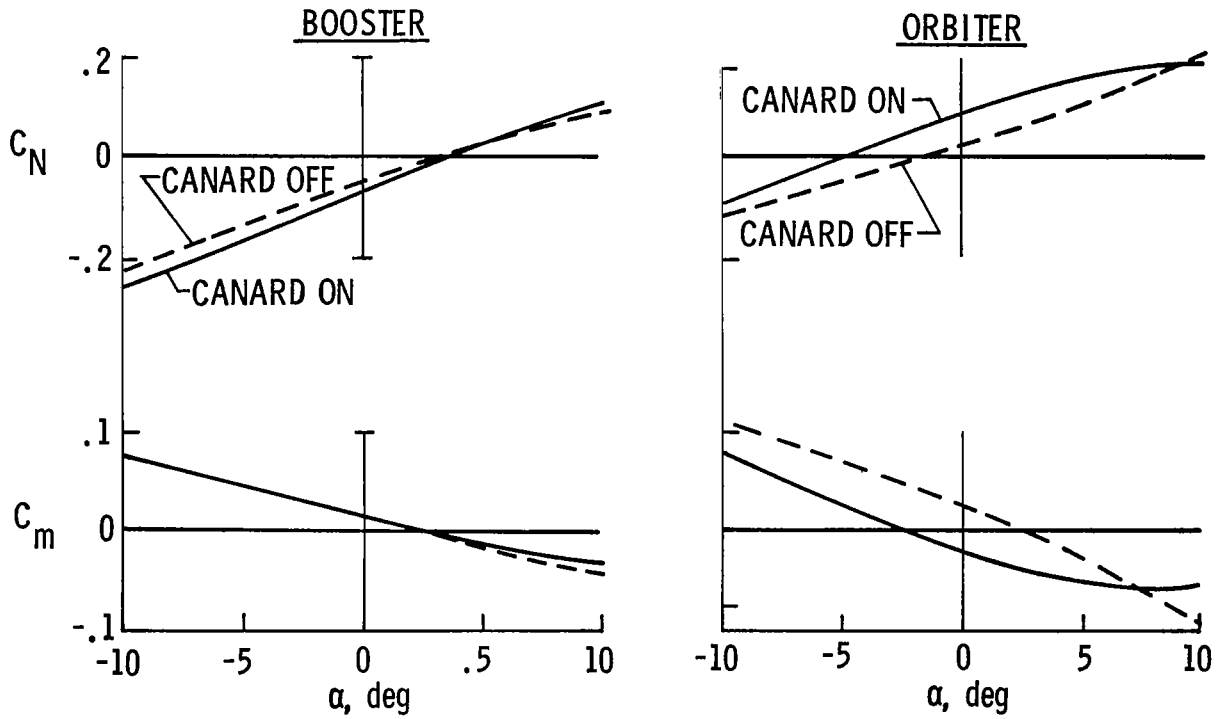

Figure 13

EFFECT OF INTERFERENCE AERODYNAMICS

(Figure 14)

To illustrate the importance of the interference aerodynamics typical dynamic simulation outputs at Mach number of 2 are presented in this figure. The trajectory data shown is with the orbiter power at 100% and the booster power at 50% at release. This would require the throttling of the 12 booster engines to 50%. The data on the left is a trajectory generated using the interference aerodynamics with plume simulation in the dynamic simulation program. The various pictures are shown at 1 second intervals from a release condition. The angle of attack and incidence angle at release were 0° and after 6 seconds the two vehicles are separating from each other. The data on the right is for a trajectory generated using just interference free aerodynamic data with plume simulation in the dynamic simulation program and for the same initial conditions. After about 3 seconds for this trajectory the two vehicles have collided. Consequently, not only is it important that the proper aerodynamic interference data be used in an abort separation dynamic program to obtain meaningful results, but also the interference aerodynamics at these conditions caused the two vehicles to separate.

EFFECT OF INTERFERENCE AERODYNAMICS

$M = 2; \alpha = 0°; \alpha_j = 0°$

ORBITER POWER = 100%; BOOSTER POWER = 50%

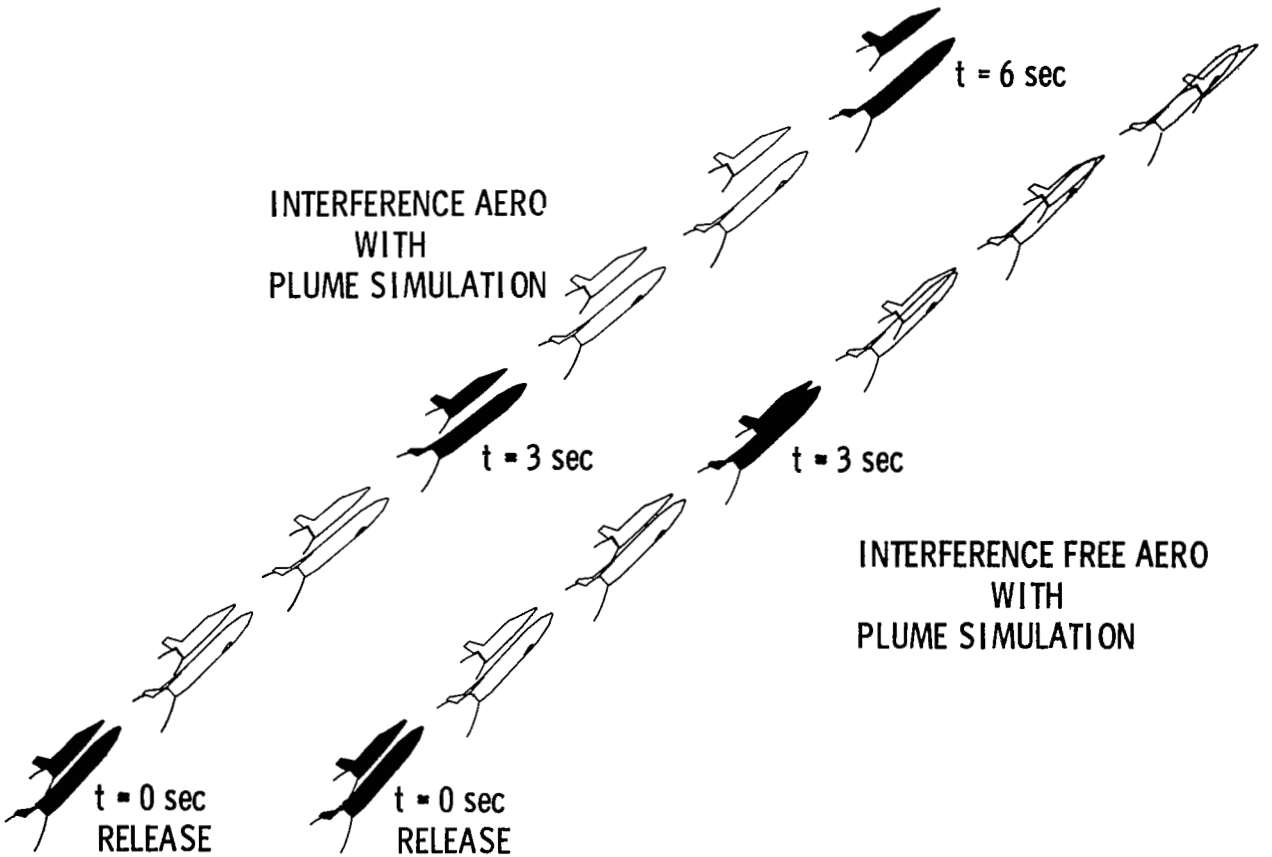

Figure 14

ROCKET EXHAUST INTERFERENCE EFFECTS

(Figure 15)

Figure 11 had shown that a large region of interference was caused by the rocket exhaust of the orbiter on the booster at M = 2. To illustrate how significant the rocket exhaust interferences were, some representative trajectories at Mach = 2 are shown. The trajectory on the left was obtained using aerodynamic wind tunnel data without the plume simulation in the dynamic simulation program while the data on the right was obtained using aerodynamic wind tunnel data with plume simulation in the dynamic simulation program. In both cases, however, the rocket thrust was included in the simulation. Both trajectories are very close to being the same. Consequently, the rocket exhaust impingement of the orbiter on the booster was not significant at the altitude and pressure ratio corresponding to the Mach number for which the rocket exhaust was simulated (see figures 4, 7, and 8). Future plume simulation would not be required if the rocket exhaust simulated in future testing generates the same size and shape plume as the rocket engines simulated at these conditions.

ROCKET EXHAUST INTERFERENCE EFFECTS

$M = 2; \alpha = 0°; \alpha_i = 0°$

ORBITER POWER = 100%; BOOSTER POWER = 50%

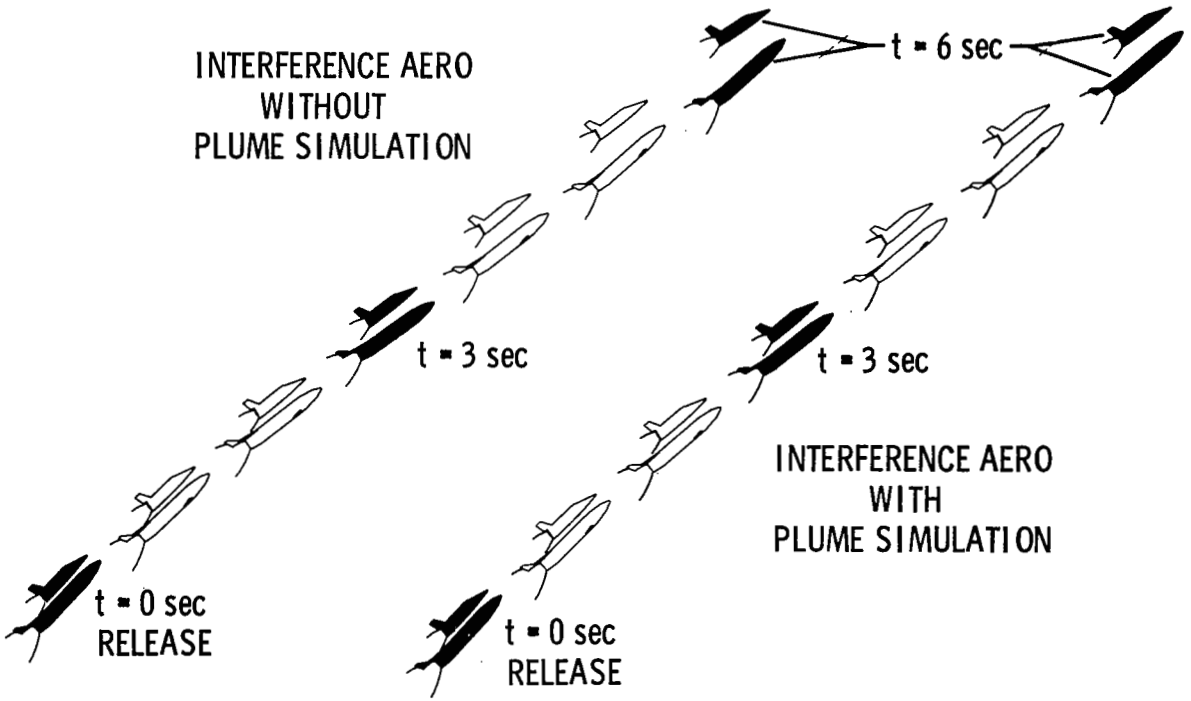

Figure 15

ROCKET EXHAUST INTERFERENCE EFFECTS

(Figure 16)

This figure shows the same type of results at M = 3 as was illustrated in figure 15 at M = 2. The data illustrated in this figure indicates that the orbiter plume impingement effects are important at the altitude and corresponding pressure ratio for which the rocket exhaust was simulated at this Mach number, since the trajectories are completely different when the aerodynamic wind tunnel data with and without plume simulation was used in the computer program. Consequently, future plume simulation would be required if the rocket exhaust simulated in future testing generates about the same size and shape plume as the rocket engines simulated at these conditions.

ROCKET EXHAUST INTERFERENCE EFFECT

$M = 3; \alpha = 0°; \alpha_i = 0°$

ORBITER POWER = 100%; BOOSTER POWER = 50%

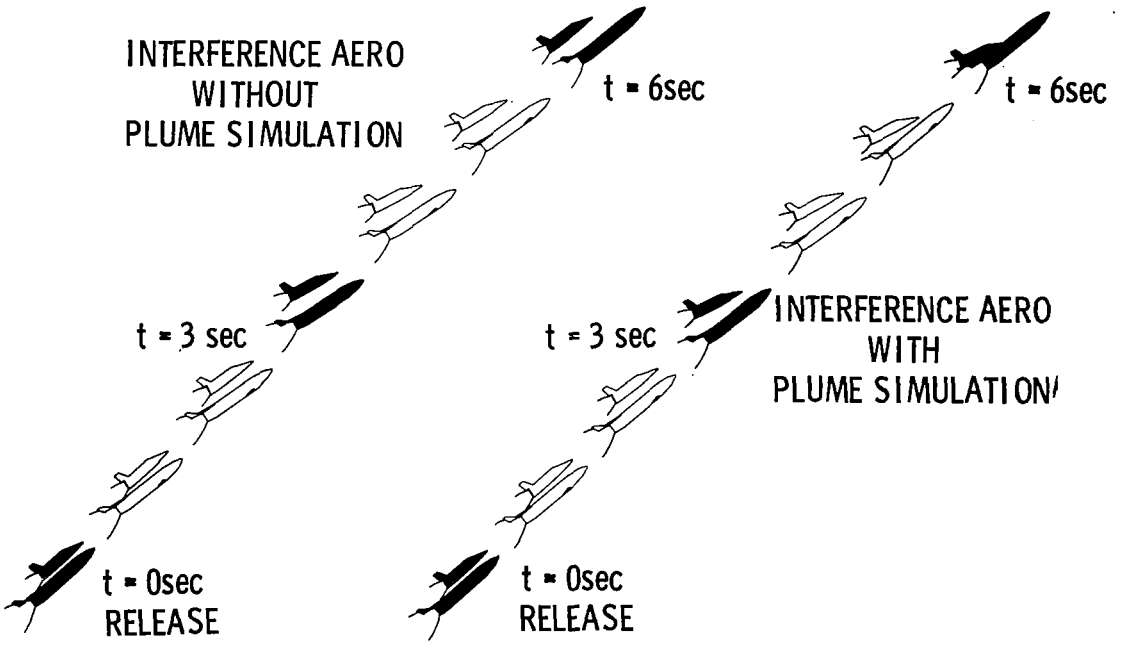

Figure 16

CONTROL EFFECTIVENESS

(Figure 17)

During the static wind tunnel tests some aerodynamic control effectiveness information was obtained for both the orbiter and booster. These results are summarized in this figure. It was found that both vehicles had control effectiveness even when in proximity to the other vehicle except for the booster at the higher Mach numbers when at interference free conditions the control effectiveness parameter, $C_{m_{\delta_e}}$, approached zero. The significance of the vehicles having control effectiveness at the lower Mach numbers is illustrated in figures 18 and 19.

CONTROL EFFECTIVENESS

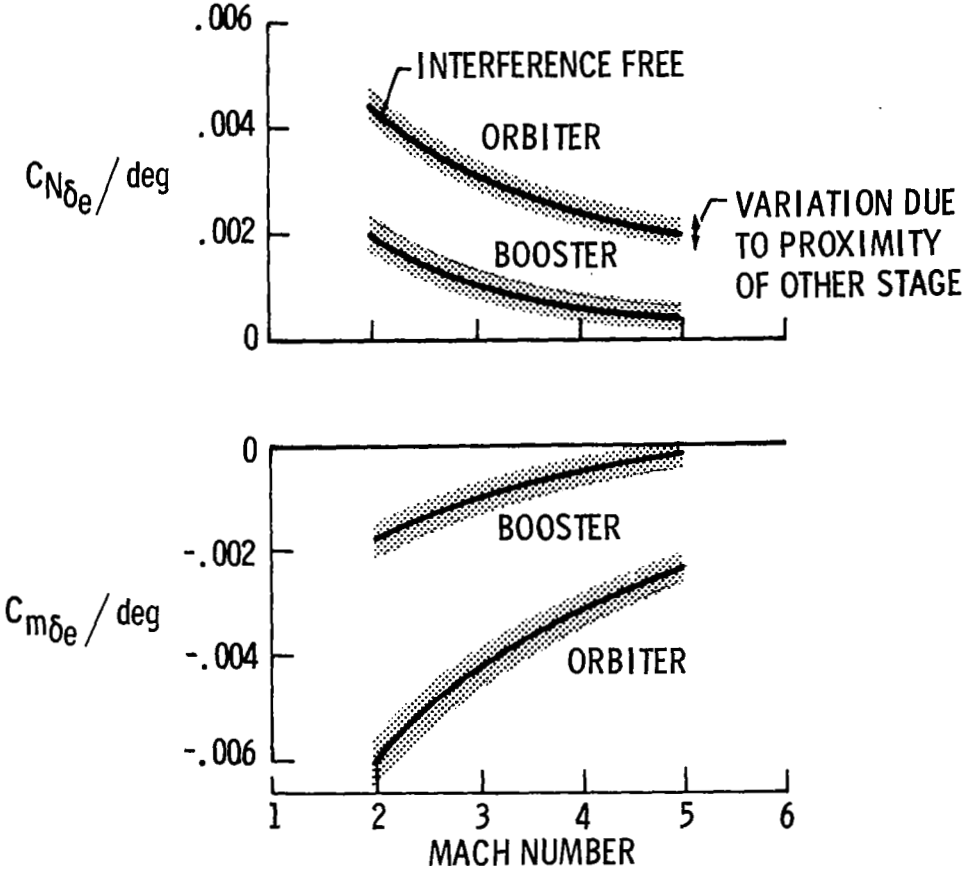

Figure 17

EFFECT OF AERO CONTROL

(Figure 18)

The importance of the aerodynamic control effectiveness for the orbiter is illustrated in this figure. The trajectory data illustrated is for a M = 2 condition and with the orbiter power level at 100% and the booster power level at 50% at release. For the case where the orbiter and booster controls are set at zero degrees it is seen that the vehicles collide after about 8 seconds. Deflecting the orbiter controls to -25° at release safely separates the vehicles at this condition.

EFFECT OF AERO CONTROL

$M = 2; \alpha = 0°; \alpha_i = 5°$

ORBITER POWER = 100%; BOOSTER POWER = 50%

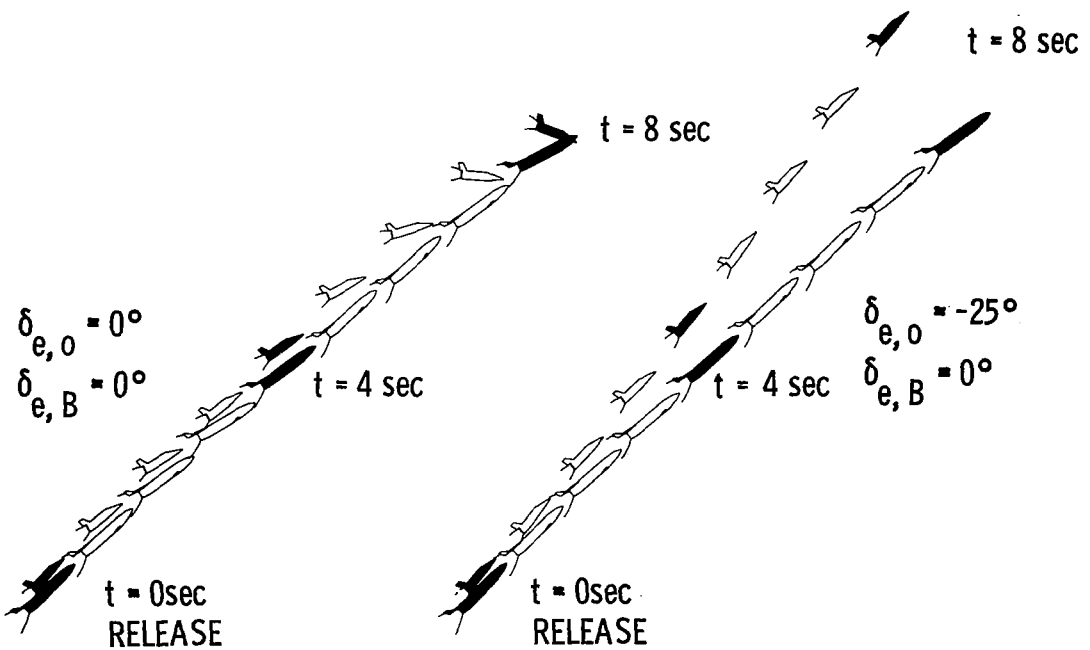

Figure 18

EFFECT OF AERO CONTROL

(Figure 19)

The importance of the aerodynamic control effectiveness for the booster is illustrated in this figure. The trajectory data shown is for a Mach number 3 condition and with the orbiter power level at 100% and the booster power level at 50% at release. For the case where the orbiter and booster controls are set at zero degrees it is seen that the vehicles collide after about 6 seconds. Deflecting the booster controls to 30° at release safely separates the vehicles at this condition.

EFFECT OF AERO CONTROL

$M = 3; \alpha = -5°; \alpha_i = 5°$

ORBITER POWER = 100%; BOOSTER POWER = 50%

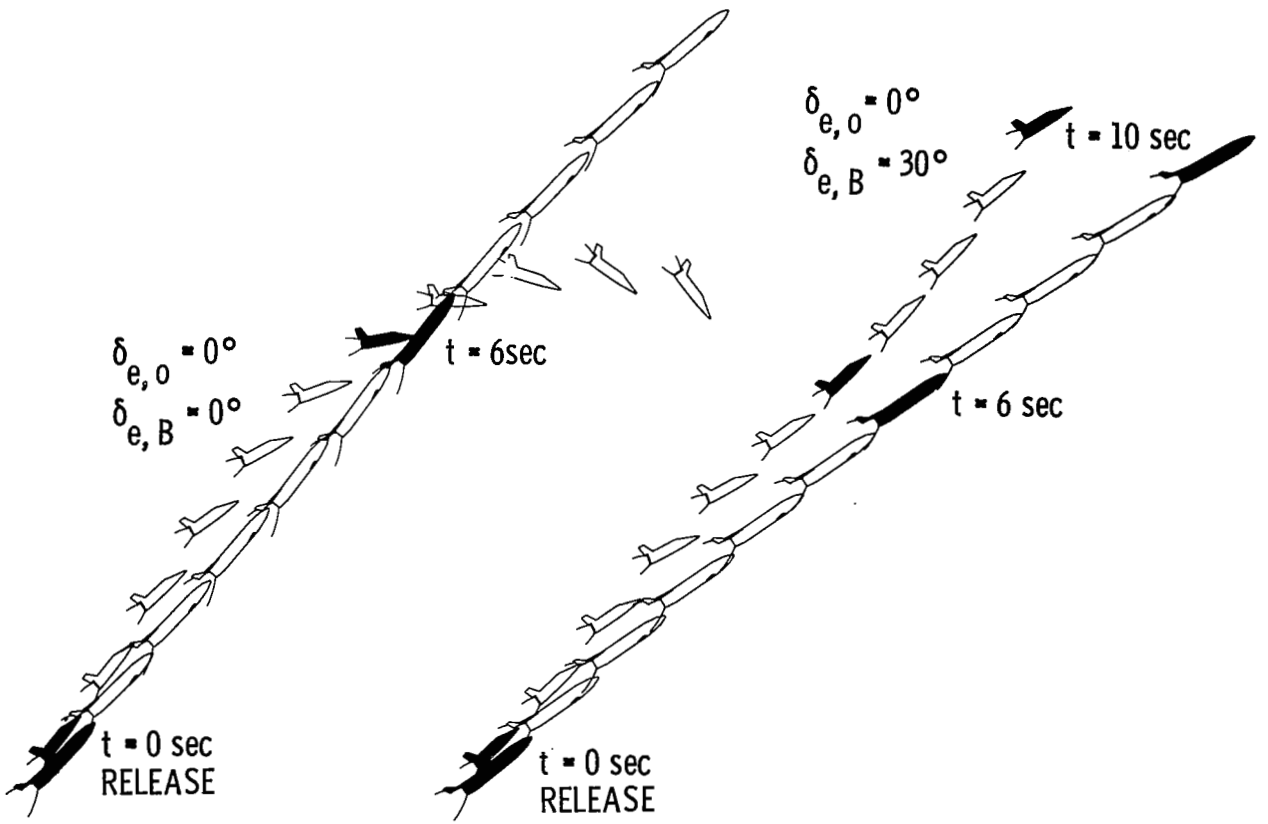

Figure 19

EFFECT OF THRUST VECTOR CONTROL ON BOOSTER

(Figure 20)

The use of thrust vector control in separating the vehicles is illustrated in this figure. This is a Mach number 5 condition with the orbiter power level at 100% and booster power level at 25% at release. Reducing the power level of the booster to 25% would require shutdown of 6 booster engines and throttling of the remaining 6 engines to 50%. As was shown in figure 17 the booster had very little aerodynamic control effectiveness at these higher Mach numbers and this would be a reason for utilizing the gimbal angle capability of the booster engines to safely separate the vehicles. For the case where the booster gimbal angle is set at 0° the two vehicles collide after about 5 seconds. However, gimbaling the booster engines to 2.5° at release allows the vehicles to safely separate. Although data is not presented in this paper for gimbaling the orbiter engines or for using the reaction control system on both the orbiter and booster, these control devices would also be useful in separating the vehicles.

EFFECT OF THRUST VECTOR CONTROL ON BOOSTER

$M = 5; \alpha = 0°; \alpha_i = 5°$

ORBITER POWER = 100%; BOOSTER POWER = 25%

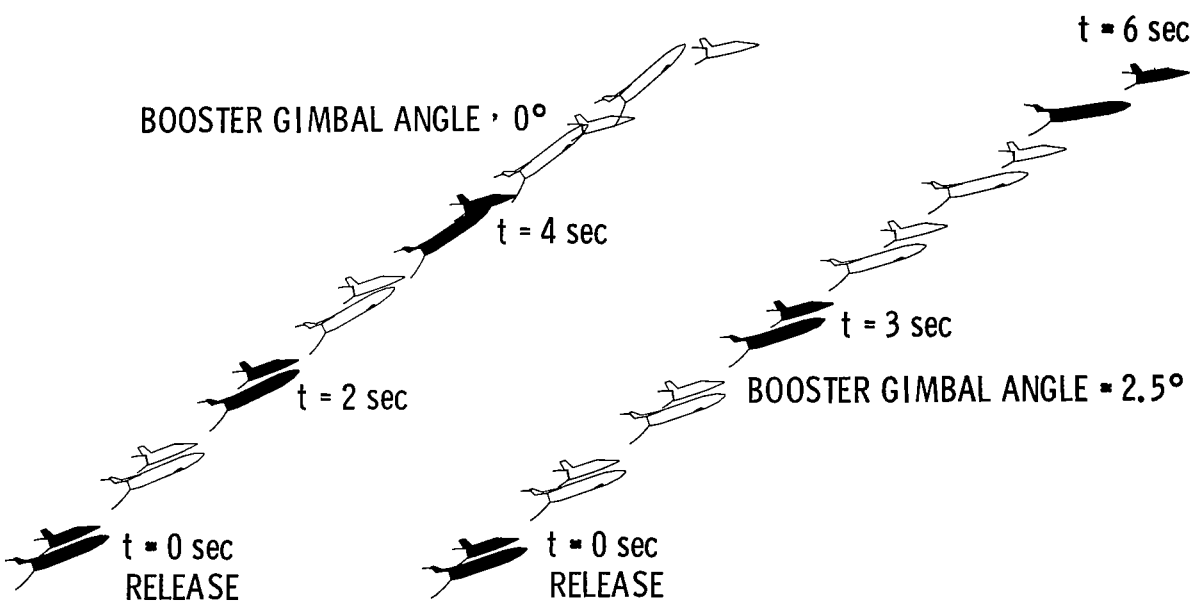

Figure 20

PITCHING MOMENT EQUATION

(Figure 21)

When considering the motion of a vehicle it is important to account for all factors which may influence the motion. The total pitching moment acting on a vehicle is composed of the sum of three distinct terms. The thrust term accounts for the canting of the thrust vector with respect to center of gravity and once the thrust level is known, the contribution to the total pitching moment is known. The static moment is also a known quantity which can be obtained from wind tunnel tests. If two bodies are involved as in the abort separation of the shuttle, this information is still obtainable from wind tunnel experiments. When the present study was started no information had been obtained on the dynamic damping contribution to the total pitching moment equation. Previous work was restricted to a single body and not two bodies in proximity to each other. The dynamic damping term plays a significant role mainly at the lower Mach numbers due to the velocity influence on the total moment. Because of a high degree of uncertainty with the dynamic damping contribution, investigations were initiated to determine if the dynamic damping term of either the orbiter or booster changed significantly when in proximity to the other vehicle.

PITCHING MOMENT EQUATION

$$M_Y = \frac{1}{2}\rho V_c^2 Sc\left(\underbrace{\frac{d_T}{c}C_T}_{\text{THRUST CONTRIBUTION}} + \underbrace{C_m}_{\text{STATIC MOMENT CONTRIBUTION}} + \underbrace{\frac{c}{2V_c}C_{m_{\dot\theta}}\dot\theta}_{\text{DAMPING-IN-PITCH CONTRIBUTION}}\right)$$

TOTAL MOMENT

Figure 21

DYNAMIC STABILITY TESTS

(Figure 22)

These dynamic stability investigations, described in more detail in paper no. 31 by K. J. Orlik-Rückemann, J. G. LaBerge, and E. S. Hanff, are illustrated in this figure. Tests were conducted at the Arnold Engineering Development Center at M = 2 on the North American Rockwell/General Dynamics Phase B delta wing space shuttle concept, reference 23, at the National Aeronautical Establishment, Canada at M = 1.8 on the North American Rockwell/General Dynamics straight wing space shuttle concept, reference 24, and at the National Aeronautical Establishment at M = 1.8 on the McDonnell-Douglas Phase B space shuttle concept, references 25 and 26. In the early portion of these tests either the orbiter or booster would be fixed and the other vehicle would be oscillated to obtain the damping-in-pitch derivative. Conducting the experiment in this fashion indicated that the interference effects on the damping-in-pitch derivative of either the orbiter or booster due to the stationary presence of the other vehicle were relatively small. However, when both vehicles were oscillated the damping-in-pitch derivative changed significantly when a phase shift occurred between the orbiter and booster. The largest increase and largest decrease in the damping-in-pitch parameter occurred when the orbiter and booster were out of phase with each other by 90° and 270° respectively. Most of the separation trajectories obtained during the present study showed that both the orbiter and booster were almost in phase with each other and oscillating with the same frequency.

DYNAMIC STABILITY TESTS

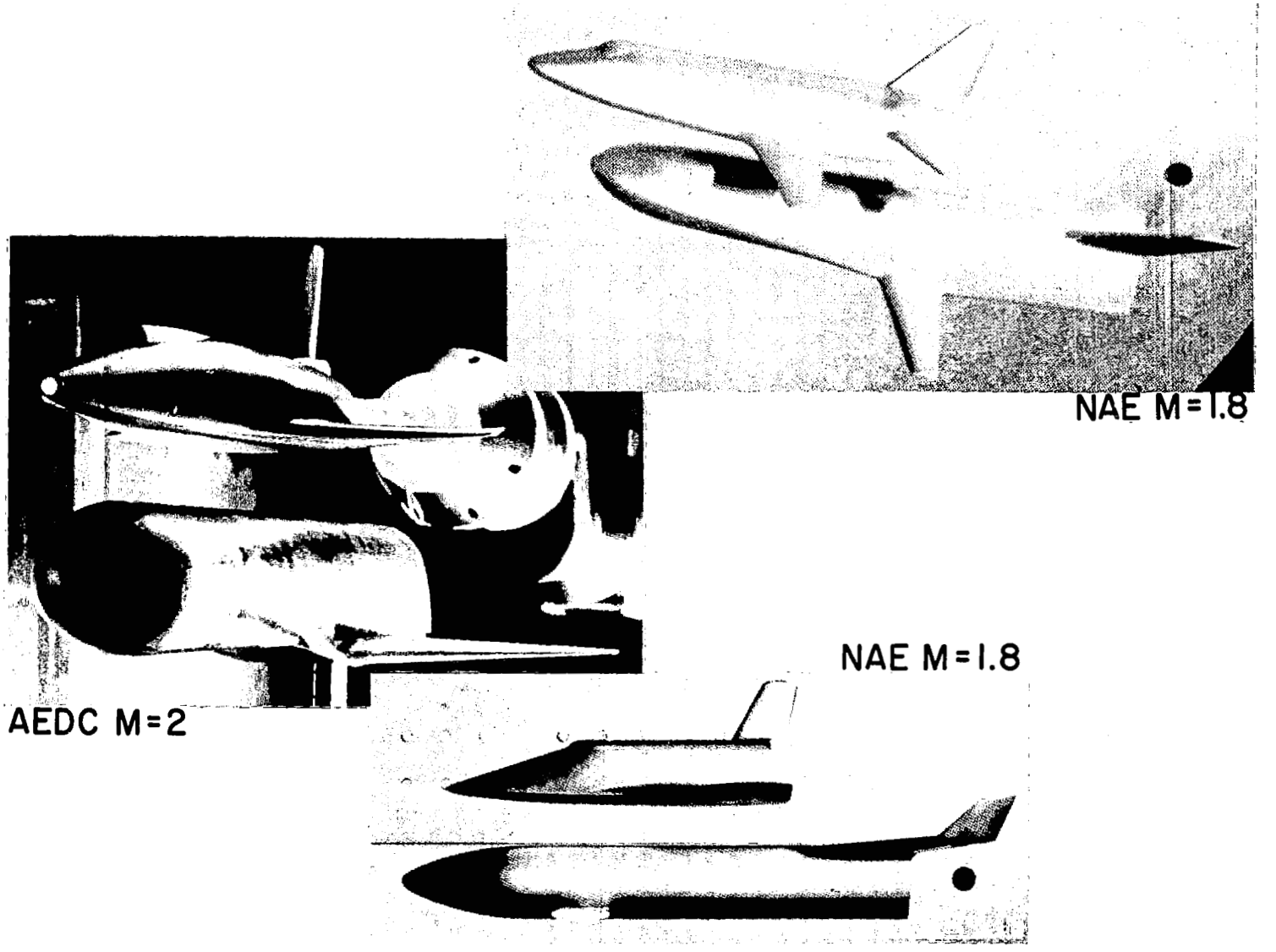

Figure 22

EFFECT OF DYNAMIC DAMPING DERIVATIVES

(Figure 23)

The implication of the change in magnitude of the damping-in-pitch derivative is illustrated in this figure. The results illustrated are at a Mach number of 2 and with the orbiter power at 100% and the booster power at 50% at release. The trajectory on the left is with the controls set at 0° deflection and with nominal values of the damping in pitch parameter for both the orbiter and booster. As can be seen, the vehicles are separating from each other after about 10 seconds. The trajectory in the center is again with the controls on the booster and orbiter set at 0° but with the damping in pitch parameters for both the orbiter and booster increased to -40/rad. It is seen here that the vehicles collide after 5 seconds. The fact that the damping-in-pitch parameter can be increased does not mean that the vehicles cannot be safely separated. Instead this is a fact for which a workable abort solution may have to be designed To illustrate this, the abort trajectory on the right is for the damping in pitch parameters for the orbiter and booster still increased to -40/rad. To safely separate the vehicles, however, the orbiter controls are set to -20° and the booster controls to +20°. Consequently, it is important to know the interference effects on the damping-in-pitch derivatives. However, as was illustrated in this figure, a safe abort separation can be obtained by properly using controls already envisioned for the vehicles.

EFFECT OF DYNAMIC DAMPING DERIVATIVES

$M = 2$; $\alpha = 0°$; $\alpha_i = 0°$

ORBITER POWER = 100%; BOOSTER POWER = 50%

$\delta_{e,o}$	= 0°	0°	-20°
$\delta_{e,B}$	= 0°	0°	20°
$\left(C_{m_{\dot{\theta}}}\right)_o$	= -3/ rad	-40/ rad	-40/ rad
$\left(C_{m_{\dot{\theta}}}\right)_B$	= -1/ rad	-40/ rad	-40/ rad

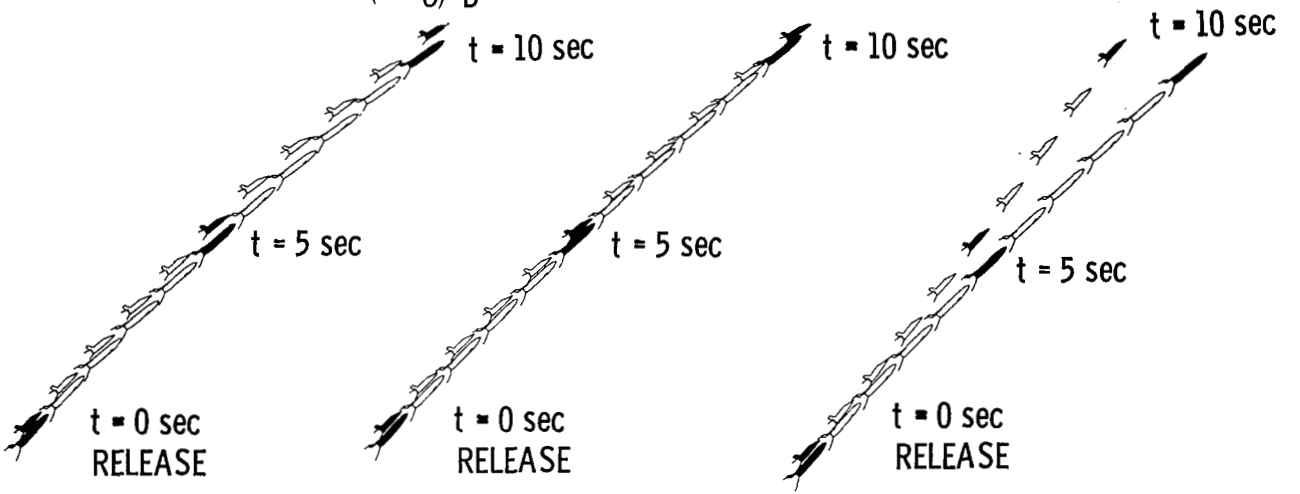

Figure 23

EFFECT OF SEPARATION MECHANISM

(Figure 24)

The potential effect of designing a separation mechanism to impart certain rotational motions to the vehicles at release is illustrated in this figure. The trajectory data on the left is for no pitch rotation imparted to the vehicles at release and it is seen that the two vehicles collide after about 4 seconds. The trajectory data on the right is for a condition where the separation mechanism has imparted a nose up pitch rotation to the orbiter of 6 deg/sec and a nose down pitch rotation to the booster of -6 deg/sec. It is seen that a safe separation trajectory is obtained.

EFFECT OF SEPARATION MECHANISM

$M = 5; \alpha = 0°; \alpha_i = 0°$

ORBITER POWER = 100%; BOOSTER POWER = 50%

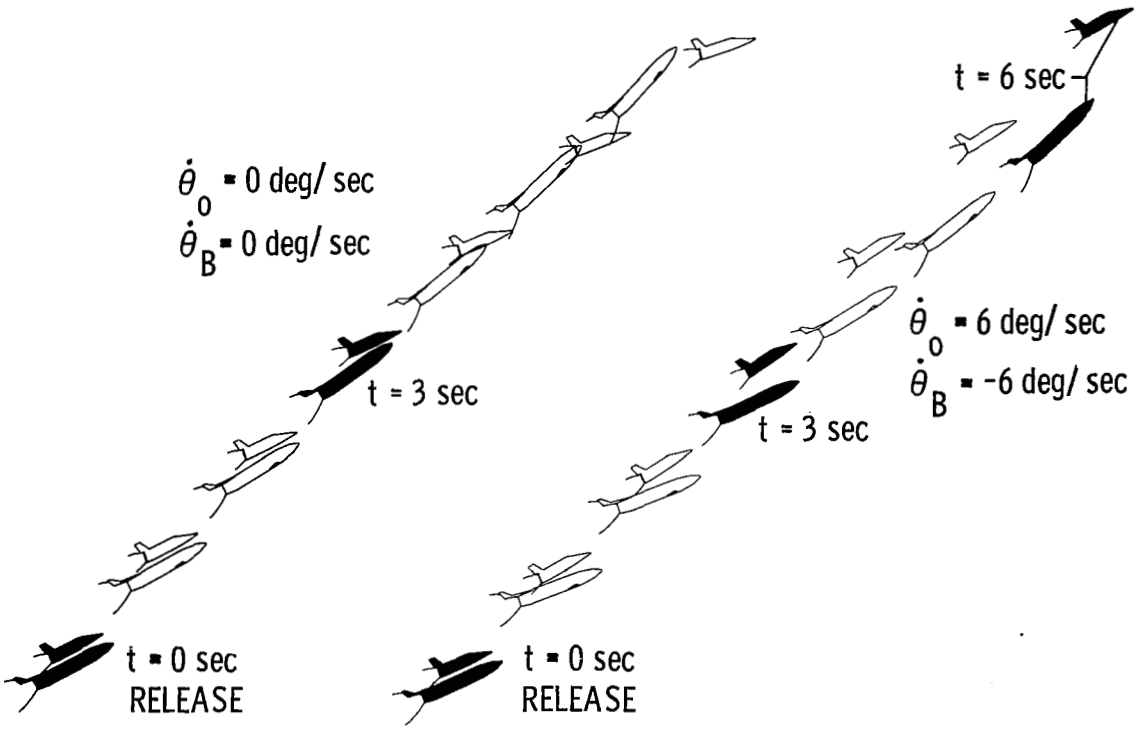

Figure 24

EFFECT OF ORBITER LOCATION

(Figure 25)

The dependency of abort separation trajectories on the location of the orbiter on the booster is shown in this figure at M = 2. One trajectory is for the nominal launch position and the other is for a parallel burn launch position. A safe abort separation is obtained when the vehicles are separated from the nominal launch position and the vehicles collide when they are separated from the parallel burn launch position. This does not imply that the nominal position is a better position than the parallel burn position since safe separation trajectories have been obtained from this position also. Instead it indicates that separation is a function of position of the orbiter on the booster.

EFFECT OF ORBITER LOCATION

$M = 2; \alpha = 0°; \alpha_i = 0°$

ORBITER POWER = 100%; BOOSTER POWER = 50%

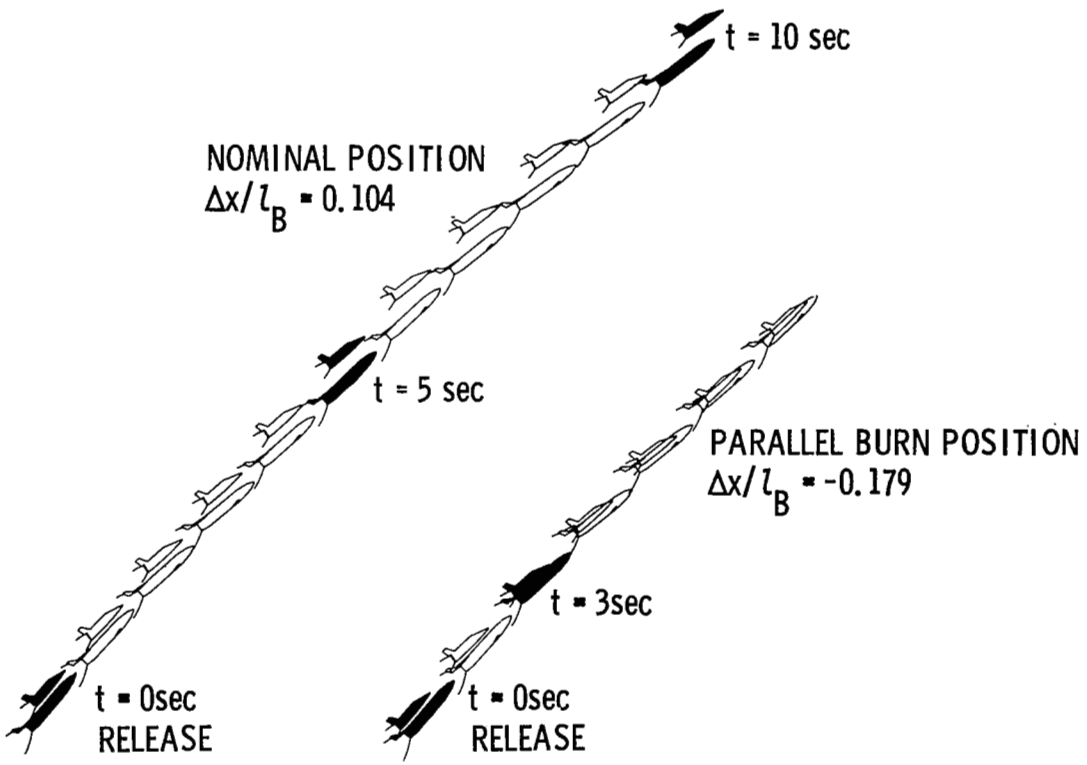

Figure 25

TECHNOLOGY IMPLICATIONS
(Figure 26)

As a result of the study to date, some observations pertinent to future studies are made.

Approach to Study Abort Staging

Close Coordination Between Technical Disciplines.- Aerodynamic staging testing could be extremely costly if the project is not well organized due to the complexity of testing and the data volume required. It is imperative that close coordination be maintained between the various technical disciplines during planning and conducting the test and during data analysis to reduce the cost and to insure that optimum use of the data is obtained.

Since the propulsion simulation requires matching of Mach number and altitude (so that the proper plume size and shape is obtained) the nominal trajectory for the system to be investigated should be well established. If excursions from the nominal trajectory are expected to be large then additional tests would be required to determine altitude effect.

Obtain Data by Grid Method.- In order to gain maximum utilization from the data, the method of obtaining aerodynamic coefficients as a function of a grid position and attitude is preferred. The captive trajectory approach might be desirable after vehicle design is firmed, but during the design phase, this approach limits data usability since only one unique trajectory can be obtained or at least a limited number fixed to certain trajectory and mass conditions.

In order to minimize amount of testing and to assure that most important interference regions are included, detailed layouts of the models and their estimated shock and plume boundaries should be made. Grid densities will then be a function of Mach number and relative location of the vehicle components such as nose, wing, canard, etc.

Automated Data Acquisition.- Completely automated data acquisition equipment which gets the man out of the loop is necessary to insure that the quantities of data required for abort analysis can be obtained quickly, efficiently, and economically. The system should be capable of automatically positioning the models at as many grid points as possible at a given set of tunnel conditions.

Another facet of data acquisition is the importance of reducing the data to orderly arrays that are amenable to being used in flight mechanic programs, plotting programs, and other programs which may be necessary for use in analysis or application of scaling parameters. The volume of data obtained from these type tests is so massive that it is prohibitive to take a manual approach or fragmented computerized approach in analysis and dissemination of test results. As much as possible, data handling analysis and dissemination should be done with computers through a totally integrated approach.

Flow Visualization.- Because of the complex flow fields caused by shock interaction and engine plume interference, analysis and understanding of resulting force and moment data requires the use of extensive flow visualization. Schlierens, shadowgraphs or interferograms should be obtained for as many conditions as practical.

Technology Concerns

Plume Simulation.- The method used to simulate the rocket exhaust of the orbiter and booster in the present study appears to be adequate. However, there are certain gray areas which need clarification to ascertain the degree of sophistication required in the simulation. Tests are needed to evaluate the effect of hot flow, momentum match and multiple nozzle arrangements.

Wind Tunnel Facilities.- For a shuttle system such as considered during the present investigation, certain facility improvements would be needed to provide final design aerodynamic data. A fully automatic twelve degree of freedom system would be desirable; however, a system which only has mixed automatic-manual capability would be acceptable for operation under a grid data acquisition mode. Although only the longitudinal motion was studied in-depth in the present study, a captive trajectory system which has eleven or twelve degrees of motion would be desirable in evaluating the out-of-plane forces and moments as they influence the separation trajectories. Definitely more degrees of motion need to be simulated in future testing.

Support hardware is needed to minimize strut and sting interference effects. For instance a ceiling or floor-mounted mechanism might be required for extreme forward orbiter to booster positions while conventional sting mounts might be acceptable for other positions.

Reynolds Number Scaling.- When conducting wind tunnel tests where the rocket exhaust is simulated, tunnel operating pressures are low to provide the back pressure necessary for the proper plume simulation. This can be minimized by using high engine model chamber pressures but only within limits of structural integrity and simulated gas supply pressures. Low tunnel pressure, however, is opposite to that desired when considering Reynolds number scaling. This can result in laminar boundary layers on the model in areas where shocks of one vehicle intersect another.

Although during this investigation we saw no adverse effects such as major flow separation, there have been other investigations where this did occur, references 27 - 30. Also, the magnitude of the effect of shocks intersecting a laminar boundary layer is unknown. The sensitivity of these effects, once obtained, needs to be assessed as they influence the abort separation trajectories.

TECHNOLOGY IMPLICATIONS

APPROACH TO STUDY ABORT STAGING

- CLOSE COORDINATION BETWEEN TECHNICAL DISCIPLINES
- OBTAIN DATA BY GRID METHOD
- AUTOMATED DATA ACQUISITION
- FLOW VISUALIZATION

TECHNOLOGY CONCERNS

- PLUME SIMULATION
  - HOT FLOW
  - MULTI-NOZZLE
  - MOMENTUM MATCH
- WIND TUNNEL FACILITIES
  - 12-DEGREE OF MOTION SIMULATION (CAPTIVE AND GRID)
  - SUPPORT HARDWARE TO MINIMIZE STING EFFECTS
- REYNOLDS NUMBER SCALING

Figure 26

CONCLUDING REMARKS

(Figure 27)

Abort separation investigations have been conducted at Mach numbers from 2 to 6 and at both high and low dynamic pressures. The investigations have included static stability, dynamic stability, and pressure distribution tests. Both the static stability and pressure distribution tests were conducted simulating the rocket exhaust from both the orbiter and booster. The data from these investigations have been utilized in a dynamic simulation program which calculates the motion of the vehicles during an abort separation maneuver. Within the scope of this study, parallel abort separation appears possible at both high and low dynamic pressures. In this study only rigid body aerodynamic data was obtained and consequently such things as scale effects and aeroelastic effects need to be considered.

Both aerodynamic and thrust vector control have been shown to be useful as an aid in the separation of the two stages. Other types of control devices such as the reaction control system for the orbiter and booster, although not considered in the present study, should also be useful to separate the vehicles. Consequently, the flight control systems presently envisioned for the shuttle vehicles appear adequate to separate the vehicles during abort conditions.

The results of this study confirm that abort separation is dependent on configuration, Mach number, rocket exhaust impingement, and relative position and attitude of the stages. Furthermore, abort separation procedures will not just depend on the configuration selected but also the concept selected.

Many different concepts are presently being considered for the shuttle system. However, the testing technology developed during this study as well as the dynamic simulation program is applicable to the separation problems for any of these concepts - for example, the separation of the external HO tank from the orbiter and even the HO tank-orbiter combination from the booster. Consequently, the abort separation methodology developed during this study is applicable to current shuttle concepts.

CONCLUDING REMARKS

- WITHIN THE SCOPE OF THIS STUDY, PARALLEL ABORT SEPARATION APPEARS POSSIBLE AT BOTH HIGH AND LOW DYNAMIC PRESSURES
- FLIGHT CONTROL SYSTEMS PRESENTLY ENVISIONED FOR THE SHUTTLE VEHICLES APPEAR ADEQUATE TO SEPARATE THE VEHICLES DURING ABORT CONDITIONS
- THE RESULTS OF THIS STUDY CONFIRM THAT ABORT SEPARATION IS DEPENDENT ON CONFIGURATION, MACH NUMBER, ROCKET EXHAUST IMPINGEMENT, AND RELATIVE POSITION AND ATTITUDE OF THE STAGES
- THE ABORT SEPARATION METHODOLOGY DEVELOPED DURING THIS STUDY IS APPLICABLE TO CURRENT SHUTTLE CONCEPTS

Figure 27

REFERENCES

1. Donaldson, J. C.: Aerodynamic Interference Effects of Parallel Delta Wings and Cone-Cylinder Bodies in Close Proximity: Force Tests at Mach Numbers 2, 5, and 10. AEDC-TDR-64-135, U.S. Air Force, July 1964. (Available from DDC as AD 351 435.)

2. Sayano, S.; Erickson, C. R.; and Murphy, J. S.: Aerodynamic Interference Associated With Two Parallel Bodies in Close Proximity in Hypersonic Flow. AFFDL-TR-64-158, U.S. Air Force, Dec. 1964. (Available from DDC as AD 357 000.)

3. Donaldson, J. C.: Aerodynamic Interference Effects of Parallel Delta Wings and Cone-Cylinder Bodies in Close Proximity: Pressure Tests at Mach Numbers 5 and 10, Heat-Transfer Tests at Mach Number 10. AEDC-TDR-64-172, U.S. Air Force, Sept. 1964. (Available from DDC as AD 353 390.)

4. Spurlin, C. J.: Aerodynamic Interference Effects of Delta Wings in Close Proximity: Pressure Tests at Mach 8. AEDC-TR-66-215, U.S. Air Force, Nov. 1964. (Available from DDC as AD 376 887.)

5. Decker, John P.; and Pierpont, P. Kenneth: Aerodynamic Separation Characteristics of Conceptual Parallel-Staged Reusable Launch Vehicles at Mach 3 to 6. NASA TM X-1051, 1965.

6. Decker, John P.: Aerodynamic Abort-Separation Characteristics of a Parallel-Staged Reusable Launch Vehicle From Mach 0.60 to 1.20. NASA TM X-1174, 1965.

7. Decker, John P.: Experimental Aerodynamics and Analysis of the Stage Separation of Reusable Launch Vehicles. Conference on Hypersonic Aircraft Technology, NASA SP-148, 1967, pp. 63-77.

8. Jones, Jerry H.: Force Tests on the Two Stages of an Aerospace Plane Configuration as the Stages Separated at Mach 3. AEDC-TR-67-45, U.S. Air Force, May 1967. (Available from DDC as AD 380 971.)

9. Decker, John P.; and Gera, Joseph: An Exploratory Study of Parallel-Stage Separation of Reusable Launch Vehicles. NASA TN D-4765, 1968.

10. Jenson, Richard; Dahlem, Valentine, III; and Schnabel, Charles W.: Hypersonic Aerodynamic Interference Analysis of Parallel Staged Blunt Delta Wings. AFFDL-TR-68-116, U.S. Air Force, Nov. 1968.

11. Matthews, M. L.: Stage Separation of Two Stage Reusable Vehicles. Doc. No. D2-90661-1, Boeing Co., July 15, 1965.

12. Decker, John P.: An Exploratory Experimental and Analytical Study of Separating Two Parallel Lifting Stages of a Reusable Launch Vehicle at Mach Numbers of 3 and 6. M.A.E. Thesis, Univ. of Virginia, 1968.

13. Decker, John P.: Aerodynamic Interference Effects Caused by Parallel-Staged Simple Aerodynamic Configurations at Mach Numbers of 3 and 6. NASA TN D-5379, 1969.

14. Flaherty, Jack I.; and Dahlem, Valentine, III: A Prediction Technique for Estimating Interference Effects During a Parallel Staged Separation Maneuver at Supersonic Speeds. AFFDL-TR-70-21, U.S. Air Force, June 1970.

15. Lanfranco, M. J.: Wind-Tunnel Investigation of the Separation Maneuver of Equal-Size Bodies. J. Spacecraft Rockets, vol. 7, no. 11, Nov. 1970, pp. 1300-1305.

16. Jenke, Leroy M.; and Lutz, Ronald G.: Force Tests of a Hypersonic Recoverable Booster in Proximity to the Second-Stage Vehicle at Mach Number 10. AEDC-TR-70-70, U.S. Air Force, May 1970.

17. Decker, John P.; McGhee, Robert J.; and Pierpont, P. Kenneth: Abort Separation Including Aerodynamic, Dynamic, Propulsive, and Trajectory Influences. Space Transportation System Technology Symposium, NASA TM X-52876, Vol. I, 1970, pp. 67-97.

18. Fossler, Ivy; and Prozan, Robert: Plume Impingement During Separation of a Two-Stage Space Shuttle Vehicle. NASA Space Shuttle Technology Conference, Vol. I, NASA TM X-2272, 1971, pp. 393-421.

19. Penny, Morris M.; and Ring, Larry R.: Definition of the Preliminary Impingement Forces and Moments for the MDAC and GD/C Booster Configurations. TM 54/20-317, LMSC-HREC-D225155 (Contract NAS9-11758), Lockheed Missiles and Space Co., July 1971.

20. Andrews, C. Donald: A Space Shuttle Parallel Staging Feasibility Study in the NASA-MSFC 14 x 14-Inch Trisonic Wind Tunnel. TM 54/20-319, LMSC-HREC D225158 (Contract NAS8-20082), Lockheed Missiles & Space Co., July 1971.

21. Herron, R. D.: Investigation of Jet Boundary Simulation Parameters for Underexpanded Jets in a Quiescent Atmosphere. AEDC TR-68-108, U.S. Air Force, Sept. 1968.

22. Baker, L. Ray, Jr.: Calibration of Propulsion Simulation Nozzles for Space Shuttle Booster and Orbiter Models for the Abort/Separation Staging Experimental Program. TM 54/20-320, LMSC-HREC D225144 (Contract NAS8-20082), Lockheed Missiles & Space Co., July 1971.

23. Uselton, Bob; and Wallace, Arthur R.: Dynamic Stability Testing of Space Shuttle Configurations During Abort Separation at Mach Numbers 1.76 and 2. AEDC-TR-71-198, U.S. Air Force, Oct. 1971.

24. Orlik-Rückemann, K. J.; and LaBerge, J. G.: Dynamic Stability Experiments on Straight Wing Space Shuttle Abort Separation at M = 1.80. Lab. Tech. Rep. LTR-UA-16, Nat. Res. Counc. Can. (Ottawa), May 1971.

25. LaBerge, J. G.: Dynamic Stability Experiments on Delta Wing Space Shuttle in Abort Separation at M = 1.80. Lab. Tech. Rep. LTR-UA-17, Nat. Res. Counc. Can. (Ottawa), July 1971.

26. Orlik-Rückemann, K. J.; and LaBerge, J. G.: Dynamic Interference Effect on Dynamic Stability of Delta-Wing Shuttle in Abort Separation at M = 2.0. Lab. Tech. Rep. LTR-UA-18, Nat. Res. Counc. Can. (Ottawa), Nov. 1971.

27. Fong, Michael C.; and Ehrlich, Carl F., Jr.: Propulsion Effects on Aerodynamic Characteristics of Lifting Reentry Vehicles. AFFDL-TR-70-12, U.S. Air Force, Mar. 1970.

28. McGhee, Robert J.: Jet Plume Induced Flow Separation on a Lifting Entry Body at Mach Numbers From 4.00 to 6.00. NASA TM X-1997, 1970.

29. Strike, W. T., Jr.: Jet Plume Simulation at Mach Number 10. AEDC-TR-70-118, U.S. Air Force, Aug. 1970.

30. McGhee, Robert J.: Some Effects of Jet Pluming on the Static Stability of Ballistic Bodies at a Mach Number of 6.00. NASA TN D-3698, 1966.